Shijun Yan,[1] Fang Du,[1] Long Wu,[1] Zhihua Zhang,[1] Changjia Zhong,[1] Qing Yu,[1] Yongfu Wang,[1] Lih-Fen Lue,[2] Douglas G. Walker,[2] Justin T. Douglas,[3] and Shirley ShiDu Yan[1]

F_1F_0 ATP Synthase–Cyclophilin D Interaction Contributes to Diabetes-Induced Synaptic Dysfunction and Cognitive Decline

Diabetes 2016;65:3482–3494 | DOI: 10.2337/db16-0556

Mitochondrial abnormalities are well known to cause cognitive decline. However, the underlying molecular basis of mitochondria-associated neuronal and synaptic dysfunction in the diabetic brain remains unclear. Here, using a mitochondrial single-channel patch clamp and cyclophilin D (CypD)-deficient mice (*Ppif* $^{-/-}$) with streptozotocin-induced diabetes, we observed an increase in the probability of Ca^{2+}-induced mitochondrial permeability transition pore (mPTP) opening in brain mitochondria of diabetic mice, which was further confirmed by mitochondrial swelling and cytochrome *c* release induced by Ca^{2+} overload. Diabetes-induced elevation of CypD triggers enhancement of F_1F_0 ATP synthase–CypD interaction, which in turn leads to mPTP opening. Indeed, in patients with diabetes, brain cypD protein levels were increased. Notably, blockade of the F_1F_0 ATP synthase–CypD interaction by CypD ablation protected against diabetes-induced mPTP opening, ATP synthesis deficits, oxidative stress, and mitochondria dysfunction. Furthermore, the absence of CypD alleviated deficits in synaptic plasticity, learning, and memory in diabetic mice. Thus, blockade of ATP synthase interaction with CypD provides a promising new target for therapeutic intervention in diabetic encephalopathy.

Large epidemiological studies have demonstrated that diabetes significantly increases the risk of dementia, cognitive decline, and Alzheimer's disease (1–3). These central nervous system (CNS) complications, referred to as diabetic encephalopathy, are present in patients with type 1 and type 2 diabetes (4,5), with no effective treatment currently (6). Compared with other diabetic complications, including cardiovascular and renal failure, diabetic encephalopathy remains relatively unexplored. Investigations of the cellular basis of diabetic impairments in peripheral organs have identified abnormalities in mitochondrial dynamics, morphology, and function in a variety of cell types, including islet cells, hepatocytes, skeletal muscle cells, mononuclear blood cells, and endothelial cells (7–9). However, the implications of diabetes on mitochondrial dysfunction in the brain and its molecular basis have yet to be fully understood.

Our recent studies demonstrated that CNS neurons are highly susceptible to mitochondrial dysfunction in diabetes-affected mice (10). Here we seek to identify whether the ion channels on the mitochondrial membrane play a critical role in the pathology of mitochondria dysfunction and neuron degeneration in the diabetic brain. Several ion channels have been identified in the mitochondrial membrane: the ATP-sensitive K^+ channel (11), the mitochondrial Ca^{2+} uniporter (MCU) (12), and, a high-conductance channel, the mitochondrial permeability transition pore (mPTP) (13). These play critical roles in the regulation of intracellular Ca^{2+} homeostasis, energy production, mitochondrial morphology, and cell death (14–16). Of these mitochondrial membrane channels, mPTP opening is a trigger for mitochondrial dysfunction and cell death under pathological

[1]Department of Pharmacology & Toxicology and Higuchi Bioscience Center, School of Pharmacy, University of Kansas, Lawrence, KS
[2]Neurodegenerative Disease Research Center, Biodesign Institute, Arizona State University, Tempe, AZ
[3]Nuclear Magnetic Resonance Laboratory, Molecular Structures Group, School of Pharmacy, University of Kansas, Lawrence, KS
Corresponding author: Shirley ShiDu Yan, shidu@ku.edu.

Received 4 May 2016 and accepted 9 August 2016.
This article contains Supplementary Data online at http://diabetes.diabetesjournals.org/lookup/suppl/doi:10.2337/db16-0556/-/DC1.

conditions such as ischemic stroke (17,18), Alzheimer's disease (19,20), Ullrich congenital muscular dystrophy (21), Parkinson's disease (22,23), and others (24). In diabetes-affected cells, including β-cells (25), adipocytes (26), and skeletal muscle cells (27), cyclophilin D (CypD)–mediated mitochondrial permeability transition is involved in the dissipation of the mitochondrial inner membrane electrochemical gradient, reduction of β-cell mass, and development of insulin resistance. In addition, the mPTP is hypersensitive to Ca^{2+} in the diabetic rat heart and thereby contributes to cardiac dysfunction (28). Thus, investigation of diabetes-induced mPTP opening in brain mitochondria is highly valuable for the development of new therapeutic interventions for diabetic neurological complications, including cognitive decline. The single-channel patch clamp technique provides a direct way to determining the ion channel activities, including the channel conductance and probability of opening. Here we used the single-channel patch clamp to directly measure the abnormalities of single-channel currents in the brain mitochondria from diabetic mice.

Although mPTP has been considered as an inducible activity of profound disease relevance, the molecular identity of the mPTP is not well understood. CypD has been suggested as an important regulator based on the pharmacological and genetic determinant, showing that cyclosporine A (CsA), a CypD-specific inhibitor, was able to inhibit mPTP opening (29) and that mitochondria lacking CypD were desensitized to mPTP opening (14,15). A novel mechanism for mPTP formation involving regulation of mPTP structure and function via F_1F_0 ATP synthase–CypD interaction has recently been proposed (30–32). This newly proposed mPTP model might also provide a link between mitochondrial energy deficiency and mPTP opening, because the interaction between ATP synthase and CypD not only causes mPTP opening but also decreases the activity of F_1F_0 ATP synthase (31). These studies raise the following unexplored key questions: Does interaction between CypD and F_1F_0 ATP synthase occur under stress or disease conditions such as diabetes? If so, does blocking F_1F_0 ATP synthase–CypD interaction protect against diabetes-induced mPTP opening and mitochondrial degeneration? Is CypD-mediated mitochondrial dysfunction linked to hyperglycemia and diabetes induced synaptic alterations? Does blocking CypD-dependent mPTP restore synaptic structure and function insulted by diabetes? Thus, uncovering the mechanism by which diabetes alters this vital F_1F_0 ATP synthase/CypD-dependent mitochondrial process is essential.

Using a single-channel mitochondrial patch clamp and a newly generated CypD-deficient diabetes mouse model, we comprehensively evaluate the consequences of changes in mPTP properties and mitochondrial function associated with diabetes. We further assess whether blockade of F_1F_0 ATP synthase–CypD interaction by deletion of CypD suppresses mPTP opening and restores synaptic plasticity and cognitive function in diabetic mice. Our investigation provides new insights into the role of CypD in mitochondrial degeneration and synaptic pathology relevant to the pathogenesis of diabetes-associated dementia and cognitive decline.

RESEARCH DESIGN AND METHODS

Patient Characteristics

Postmortem brain materials from patients with diabetes and age-matched control subjects without diabetes were obtained from Banner Sun Health Institute (Sun City, AZ). Frozen and fixed human brain tissues for this study were from subjects who had enrolled in the Brain and Body Donation Program (33) at the Banner Sun Health Research Institute, which is approved by the Banner Health Institutional Review Board. All patients were given written informed consent. Detailed information for each of the subjects studied is reported in Supplementary Table 1. There was no statistically significant difference in PMI between brain tissues from healthy control subjects and from patients with diabetes.

Animals

Protocols involving animal use were approved by the University of Kansas-Lawrence Animal Care and Use Committee in accordance with the National Institutes of Health guidelines for animal care. CypD homozygous-null (*Ppif*$^{-/-}$) mice were gifts from Dr. Jeffery D. Molkentin (15). Diabetes was induced in 3-month-old wild-type (WT) or *Ppif*$^{-/-}$ male mice by intraperitoneal administration of streptozotocin (STZ) (at 50 mg/kg, freshly dissolved in 100 mmol/L sterile citric acid, pH 4.5; Sigma-Aldrich) for 5 consecutive days, as previously described (34). Metabolic features are reported in Supplementary Table 2. After 2–3 months' duration of STZ-induced diabetes, these mice were evaluated with the Morris Water Maze (MWM) test. Brains, not including the olfactory bulb and cerebellum, were dissected, weighed, and snap-frozen in liquid nitrogen or used for cortical mitochondria isolation for further analysis, as described below.

Mitochondria Isolation and Assays

Cerebral cortices and hippocampi were dissected and homogenized in cold mitochondria isolation buffer (225 mmol/L D-mannitol, 75 mmol/L sucrose, and 2 mmol/L K_2HPO_4, pH 7.2). Mitochondria were isolated by centrifugation, as previously described (10).

Mitochondrial swelling assay was performed on 100 μg of mitochondria in 1 mL of mitochondria swelling buffer (225 mmol/L D-mannitol, 75 mmol/L sucrose, 2 mmol/L K_2HPO_4, 5 μmol/L glutamate, and 5 μmol/L malate, pH 7.2). Swelling was triggered by the addition of 100 μmol/L $CaCl_2$. In some experiments, mitochondria were incubated with CsA for 5 min on ice before the swelling assay. Swelling was monitored with light scattering at 540 nm on an Ultrospec 3100 pro Spectrophotometer (Amersham Biosciences) for 12 min, including a 2-min baseline before Ca^{2+} addition.

Ca-induced cytochrome *c* release was detected in the mitochondria using previously described methods (15). Briefly, isolated mitochondria were incubated in the isolation buffer at room temperature in the presence of $CaCl_2$ with indicated concentrations for 30 min. Then the mitochondria were centrifuged at 8,000*g* for 10 min, and the resulting mitochondrial pellets and supernatant were subject to immunoblotting assay.

CypD membrane translocation (19), mitochondrial oxygen consumption rate (OCR) (19,35), and ATP synthase activity (36) were measured as previously described.

Mitochondrial Patch Clamp

Mitochondrial single-channel patch clamp was performed, as previously described (37,38), with modifications. Briefly, 5 μL solution of freshly isolated mitochondria (about 2–5 μg mitochondria) was added to the bath recording solution (150 mmol/L KCl, 20 mmol/L K-HEPES, and 1 mmol/L $CaCl_2$, pH 7.2) in a glass bottom recording chamber, which was then left undisturbed for several minutes to allow mitochondria to settle onto the bottom of the chamber. Patch pipettes were pulled in two steps from glass capillaries (World Precision Instrument) using a Narishige puller and polished by heating (Narishige) to yield a resistance of 20–50 MΩ when filled with pipette solution (150 mmol/L KCl and 20 mmol/L K-HEPES, pH 7.2). Mitochondria were approached by means of an electrically driven micromanipulator (MPC-200, Sutter Instrument). Recordings were collected using a MultiClamp 700B amplifier, a digitizer (Digidata 1440A), and pClamp 10.3 software (Molecular Devices) after obtaining a seal resistance of 1 to 2 GΩ. Single-channel currents were recorded at the fixed holding potential indicated in the respective figures. P_o represents the average channel opening probability and was determined by all-point analysis.

Immunoprecipitation and Immunoblotting Assays

For immunoprecipitation, isolated mitochondria were lysed in PBS containing 0.5% NP-40, 1 mmol/L phenylmethylsulfonyl fluoride, and protease inhibitor mixture (Calbiochem). Mitochondria lysates (1 mg/mL, 300 μL) were then incubated overnight under wheel rotation at 4°C in the presence of anti-ATP synthase antibody (Cat# ab109867; Abcam) or nonimmune IgG. Complexes were precipitated by A/G-Agarose beads (#20421; Pierce) and washed in PBS. Immunoprecipitation supernatants were separated by SDS-PAGE, followed by immunoblotting analysis. For immunoblotting assays, brain tissues, isolated mitochondrial fractions, or protein samples were homogenized in extraction buffer (10 mmol/L Tris-HCl [pH 7.4], 100 mmol/L sodium chloride, 1 mmol/L EDTA, 1 mmol/L EGTA, 1 mmol/L sodium fluoride, 20 mmol/L sodium pyrophosphate, 2 mmol/L sodium orthovanadate, 1% Triton X-100, 10% glycerol, 0.1% SDS, and 0.5% deoxycholate) containing 1 mmol/L phenylmethylsulfonyl fluoride and protease inhibitor mixture (Calbiochem).

Samples were separated under denaturing conditions on 10% SDS-PAGE and transferred to a nitrocellulose membrane (Amersham). Membranes were then incubated overnight at 4°C with primary antibodies: anti-mouse CypD (Cat# ab110324; Abcam), Rabbit anti-human CypD (generated in our laboratory) (19), Hsp60 (Cat# ADISPA806D; Enzo), *N*-methyl-D-aspartate receptor subtype 2B (NR2B) (Cat# ab28373; Abcam), postsynaptic density protein 95 (PSD95) (Cat# ab16495; Abcam), synapsin I (Cat# PA1-4673; Affinity Bioreagents), synaptophysin (Cat# MAB5258; Chemicon), cytochrome *c* (Cat# 4272s; Cell Signaling), cyclooxygenase IV (Cat#A21348; Invitrogen), or β-actin (Cat# A5441; Sigma-Aldrich). Membranes were incubated with horseradish peroxidase–conjugated anti-rabbit or anti-mouse IgG (Life Technology), visualized using enhanced chemiluminescence detection reagents (Thermo Fisher Scientific), and scanned by FluorChem HD2 (Cell Biosciences). The intensity of immunoreactive bands was quantified by ImageJ software (National Institutes of Health).

Confocal Immunostaining

Mouse brains were fixed with 4% paraformaldehyde at 4°C for 2 days after saline perfusion. Fixed brains were cut into 30-μm-thick sections on a Vibratome (Leica VT1000S). Precut free-floating temporal cortex sections (40 μm thick) of postmortem human brains were obtained from Banner Sun Health Institute (Sun City, AZ) for immunohistochemistry. The following primary antibodies were used for immunostaining: CypD (Cat# ab110324; Abcam), MAP2 (Cat# 1281959; Boehringer Mannheim), PSD95 (Cat# 16495; Abcam), synaptophysin (Cat# MAB5258; Chemicon), synapsin I (Cat# PA1-4673; Affinity Bioreagents), anti–4-hydroxy-2-nonenal (4-HNE) IgG (1:100, Abcam). Alexa Fluor 488 or 594 secondary antibodies (Invitrogen) or biotin-conjugated goat anti-rabbit IgG (Sigma-Aldrich) were used. Sections were imaged under a Leica DMI4000B confocal microscope, and images were analyzed by the Universal MetaMorph Image Program (Molecular Devices).

Imaging Studies of Pancreatic Islets and Serum Insulin Measurement

Formalin-fixed pancreas sections underwent antigen retrieval in boiling citrate buffer (pH 6.0) for 10 min before labeling with antibodies against insulin (Cat# ab7842; Abcam). Sections were incubated with horseradish peroxidase–conjugated IgG (Sigma-Aldrich), followed by staining using 3-amino-9-ethylcarbazole (AEC) substrate. Serum was collected after 6-h fasting, and insulin levels were measured by ELISA kit (Crystal Chem), following the manufacture's instruction.

Measurement of Reactive Oxygen Species by Electron Paramagnetic Resonance and MitoSOX Red Staining

We measured tissue reactive oxygen species (ROS) levels in mouse brains using electron paramagnetic resonance (EPR) assay (39,40) and MitoSOX Red (Molecular Probes) staining, as previously described (41).

Tetramethylrhodamine Methyl Ester Staining

WT or *Ppif*$^{-/-}$ hippocampal neurons were cultured from day 1 newborn mice in Neurobasal B27 media containing

25 mmol/L D-glucose (Invitrogen). Tetramethylrhodamine methyl ester (TMRM) was used to stain 12–14 day in vitro neurons, as previously described (19).

MWM and Long-term Potentiation Studies

The MWM test was performed as previously described (34). The training protocol for the hidden platform version of the MWM consisted of four trials (60-s maximum) each day for 6 consecutive days. The probe trial was done on day 7. The trajectories were recorded with a video tracking system. Investigators were blinded to mouse genotypes and treatments until the behavioral tests were finished.

We performed long-term potentiation (LTP) recordings as previously described (42,43). Slices were prepared using a chopper (Electron Microscopy Sciences) and maintained at 29°C in an interface chamber (Warner Instruments) with artificial cerebrospinal fluid containing (in mmol/L): 125 NaCl, 2.5 KCl, 2 $CaCl_2$, 1 $MgCl_2$, 1.25 NaH_2PO_4, 24 $NaHCO_3$ and 15 glucose, bubbled with 95% O_2/5% CO_2. Slices were allowed to recover for at least 1.5 h before recording. Field-excitatory postsynaptic potentials were recorded from the CA1 region of the hippocampus by placing the bipolar silver stimulating electrode at the level of the Schaeffer collateral fibers, whereas the recording electrode was placed in the stratum radium area of CA1. Extracellular responses were acquired using Clampex Software 10.4 (Molecular Devices) and a microamplifier (IE-210; Warner Instruments). LTP was induced by θ-burst stimulation (4 pulses at 100 Hz, with the bursts repeated at 5 Hz and each tetanus including three 10-burst trains separated by 15 s). Data collection and analysis were performed by investigators blinded to the experimental conditions.

Statistical Analysis

All data are expressed as means ± SEM. Statistical analysis with two-tailed Student *t* test and one-way ANOVA was performed using StatView statistics software and GraphPad Prism. Pearson correlation analysis was performed using GraphPad Prism. $P < 0.05$ was considered significant.

RESULTS

Single-Channel Patch Clamp Reveals Elevated mPTP Opening Probability in Diabetic Brain Mitochondria

To determine ion channel abnormalities in diabetes-affected brain mitochondria, we first recorded single-channel events and analyzed the difference in channel opening probability of mitochondria from STZ-administered mice versus vehicle controls. Black, well-separated, and round vesicles of ~1 μm in diameter were approached and gigasealed by pipette tip (Fig. 1*A*). In the mitochondria-attached configuration, we recorded 61 single-channel currents in vehicle-mitochondria and 45 currents in STZ-mitochondria, with detection channel conductance ranging from 100 ps to 1.5 ns. Most of them in the vehicle-mitochondria and STZ-mitochondria displayed ~250 ps (Supplementary Fig. 1*A*), 500–700 ps (Supplementary Fig. 1*B*), or large-channel conductance (>800 ps) (Fig. 1*B*). In the subgroup of channels with large channel conductance, STZ-mitochondria showed significantly increased single-channel opening probability (P_0) compared with vehicle-mitochondria, but no significant difference in P_0 was found in the subgroups of ~250 ps or 500–700 ps events (Fig. 1*C* and Supplementary Fig. 1*A* and *B*).

mPTP has been established as a high conductance ion channel with up to 1.3 ns whose opening can be induced by increased cytosolic Ca^{2+} concentrations or specifically blocked by CsA (29). According to CsA sensitivity, the large conductance channels were subdivided into two groups: mPTP, with CsA sensitivity (Fig. 1*D*) and non-mPTP channel, without CsA sensitivity (Supplementary Fig. 1*C*). Large conductance channels with CsA sensitivity displayed increased P_0 differentials between vehicle- and STZ-mitochondria (Fig. 1*E*, upper panel), but no significant difference in P_0 was observed in non-mPTP channels (Fig. 1*E*, lower panel), suggesting that enhanced mPTP opening contributes to the increased P_0 in the subgroup of large conductance channels in STZ-mitochondria. No significant difference in mPTP channel conductance was observed between vehicle- and STZ-mitochondria (Fig. 1*F*).

Interaction of F_1F_0 ATP Synthase With CypD Contributes to the Hypersensitivity of mPTP Insulted by Diabetes

mPTP regulates solute exchange between the mitochondrial matrix and the cytoplasm. Prolonged mPTP opening induced by Ca^{2+} overload leads to mitochondrial swelling and cytochrome *c* release (14,15). Consistent with patch clamping results showing increased mPTP opening, brain mitochondria from STZ diabetic mice displayed increased swelling (Fig. 2*A*) and cytochrome *c* release (Fig. 2*B*) when stimulated by Ca^{2+}, indicating that more STZ-mitochondria transform from the closed to the open state under Ca^{2+} stimulation compared with vehicle-mitochondria. In addition, CsA, the CypD inhibitor, suppressed overswelling of STZ-mitochondria in a dose-dependent manner (Fig. 2*C* and *D*). These data further illustrated the enhancement of CypD-dependent mPTP opening in diabetic mitochondria.

The enhanced mPTP opening in response to elevated Ca^{2+} led us to examine whether these changes are associated with increased expression of CypD in diabetic mitochondria. STZ mice exhibited significant elevation of CypD expression (Fig. 3*A*) by 1.5- to 2.5-fold in the hippocampus and cortex, regions related to memory formation, compared with nondiabetic littermates. Considering that increased CypD levels might be caused by increased mitochondria proliferation, we next examined the CypD levels in isolated brain mitochondria. Compared with vehicle-mitochondria, STZ-mitochondria displayed higher CypD contents (Fig. 3*B*), suggesting that it is unlikely that increased CypD expression in diabetic brain mitochondria was caused by mitochondrial proliferation. Hsp60 protein levels in mitochondrial samples from vehicle or STZ mice were comparable and thus served as a loading reference. Accordingly, in situ immunohistochemistry staining showed increased density of CypD in the hippocampus CA1 region

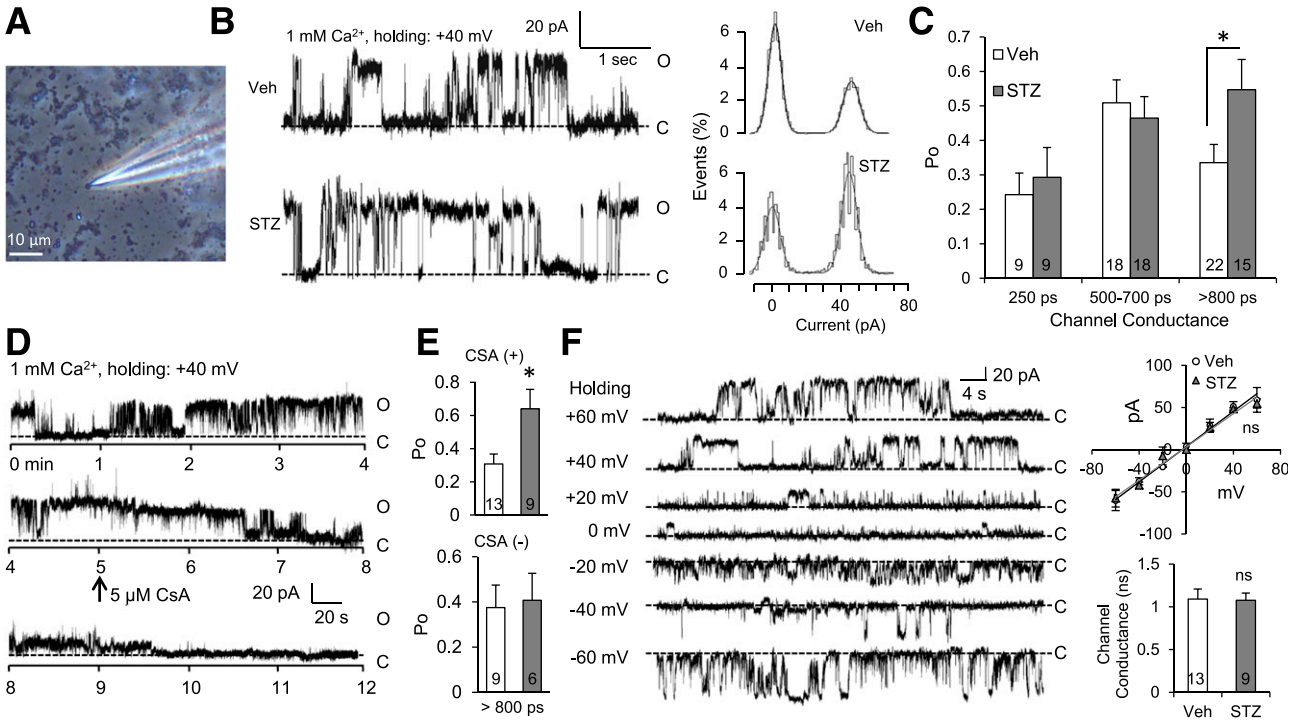

Figure 1—Effect of diabetes on ion channels in mouse brain mitochondria. *A*: Respective phase-contrast image of mitochondria patched with a micropipette. The scale bar is 10 μm. *B*: Representative single-channel current traces of a large conductance ion channel (~1.0 ns) in brain mitochondria from nondiabetic controls and STZ-induced diabetic C57BL/6 WT mice. Mitochondria were clamped at +40 mV in the presence of 1 mmol/L Ca^{2+} in bath. All-point amplitude histograms for the traces are shown in the right panel. Amplitude distributions were fitted with two Gaussian components. *C*: Average opening probability (P_0) of ion channels with various conductance in brain mitochondria with or without STZ-induced diabetes. The ratio of the area under the fitted "open" Gaussian to the total area under the entire Gaussian was taken as P_0. *D*: Representative current trace of a large conductance ion channel with CsA-sensitive activity. Mitochondria were clamped at +40 mV, and 5 μmol/L CsA was added into the bath solution containing 1 mmol/L Ca^{2+} at 5 min. *E*: Average opening probability (P_0) of large conductance ion channels with (upper panel) or without (lower panel) CsA sensitivity in vehicle or STZ-injected mice. *F*: CsA-sensitivity channels showed no difference in the channel conductance between the vehicle and STZ mitochondria. Representative single-channel current traces of the CsA-sensitive channel holding at the indicated voltages (from −60 to +60 mV with 20 mV intervals) are shown in the left panel. Current-voltage (I-V) plot was averaged from the CsA-sensitive channel recordings. Channel conductance was obtained from the I-V relationship. The "o" and "c" indicate open and closed states, respectively. Data are represented as mean ± SEM (n = 6–10 mice per group). Veh, vehicle. ns, not significant; *P < 0.05.

and cerebral cortex (Fig. 3*C*) in diabetic mice. These results demonstrate that CypD expression is increased in the diabetic brain, which likely contributes to the enhancement of mPTP opening.

The molecular nature of the mPTP remains the subject of protracted scientific debate, but progress has recently been made with the identification of the F_1F_0 ATP synthase as the pore-forming component of mPTP, which provides a novel molecular mechanism underlying the modulation of pore formation through F_1F_0 ATP synthase–CypD interaction (30,32). Enhanced mPTP opening in response to elevated Ca^{2+} and increased expression of CypD in the diabetic brain led us to examine whether these are linked by increased interaction of CypD with F_1F_0 ATP synthase. First, we examined translocation of CypD from the mitochondrial matrix to the inner membrane in response to Ca^{2+} overload. STZ-mitochondria displayed increased translocation of CypD to the mitochondrial inner membrane after Ca^{2+} (100 μmol/L) treatment (Fig. 3*D*). Second, we examined the interaction between F_1F_0 ATP synthase and CypD by coimmunoprecipitation assay using brain mitochondria. As shown in Fig. 3*E*, CypD was present in F_1F_0 ATP synthase immunoprecipitates, which is consistent with previous reports (31,32). Furthermore, the amount of CypD in F_1F_0 ATP synthase immunoprecipitates was increased in STZ-mitochondria compared with vehicle-mitochondria (Fig. 3*F*). These results suggest that the diabetes-induced elevation of CypD provides more available CypD protein for recruitment to the mitochondrial inner membrane and subsequently interacts with F_1F_0 ATP synthase, leading to mPTP formation under Ca^{2+} overload insulted by diabetes.

CypD Deficiency Prevents Diabetes-Induced Mitochondrial Dysfunction in the Diabetic Brain

Given that increased CypD interaction with F_1F_0 ATP synthase was associated with mPTP dysfunction in the brain affected by diabetes, we next determined whether CypD deficiency is able to rescue diabetes-associated mitochondria and neuronal perturbation by using *Ppif* $^{-/-}$

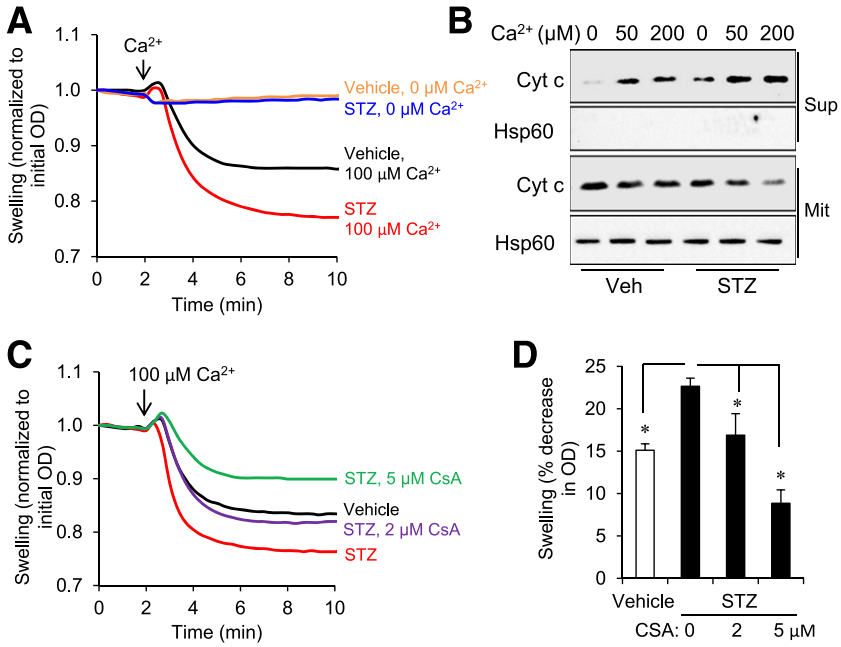

Figure 2—Hypersensitivity of CypD-regulated mPTP opening in response to Ca^{2+} overload in diabetic brain mitochondria. *A*: Traces of mitochondrial swelling induced by 100 μmol/L Ca^{2+} in vehicle or STZ mitochondria. *B*: Ca^{2+} induced cytochrome *c* (Cyt c) release. Isolated mitochondria were incubated with the indicated concentrations of Ca^{2+} for 30 min, and the resultant supernatant (Sup) and pellets (Mit) were immunoblotted for cytochrome *c* and Hsp60. Hsp60 served as a control for an equivalent amount of the mitochondrial protein loading in each sample and the mitochondrial protein marker. Similar results were observed in at least three independent experiments. *C*: Traces of mitochondrial swelling in the presence of the CypD inhibitor, CsA. *D*: Quantification of the mitochondrial swelling as shown in panels *A* and *C*, expressed as the percentage change relative to the initial optical density (OD) in the indicated mice (n = 3–4 mice per group). *$P < 0.05$.

mice. In *Ppif* $^{-/-}$ mice, the absence of CypD was verified by PCR and immunoblotting for CypD protein expression (Supplementary Fig. 2*A*–*C*). *Ppif* $^{-/-}$ mice do not have any detectable phenotypic anomalies, as we previously described (19). To validate the effect of CypD deficiency on mitochondrial membrane potential under physiological condition, we monitored TMRM signals in primary cultured hippocampal neurons derived from *Ppif* $^{-/-}$ mice by staining of live images with TMRM, a fluorescent probe widely used to measure the mitochondrial membrane potential. No significant difference in TMRM signals was observed between CypD-deficient neurons and WT neurons (Supplementary Fig. 2*D*). Blood glucose levels, body weight, β-cell loss in pancreatic islets, and serum insulin levels were comparable between WT-STZ mice and CypD-deficient STZ mice, suggesting that loss of CypD does not affect STZ-induced metabolic changes (Supplementary Table 2 and Supplementary Fig. 3).

Cortical mitochondria isolated from diabetic mice showed greater swelling induced by 100 μmol/L Ca^{2+} than normal mitochondria (Fig. 4*A*), whereas *Ppif* $^{-/-}$ mitochondria isolated from nondiabetic and diabetic mice were resistant to Ca^{2+}-induced swelling (Fig. 4*A*). No difference in Ca^{2+}-induced cytochrome *c* release from mitochondria was observed between *Ppif* $^{-/-}$ mitochondria with and without diabetes (Fig. 4*B*). In addition, mitochondria lacking CypD restored decreased F_1F_0 ATP synthase activity in STZ brains (Fig. 4*C*). We next evaluated mitochondrial function by measuring mitochondrial oxygen consumption rate (OCR). Compared with nondiabetic WT mice, STZ-treated WT mice exhibited a significant reduction in OCR, whereas STZ administration did not affect the OCR in *Ppif* $^{-/-}$ mice (Fig. 4*D*). Given mitochondrial respiratory deficits were usually accompanied by increased ROS production (44), we determined whether CypD deficiency inhibits oxidative stress in STZ mouse brains. Brain ROS levels were measured by highly selective and sensitive EPR, which detects the presence of unpaired electrons and provides an excellent technique for measuring intracellular free radicals (39,40). The peak of the EPR signal detected was considerably higher in diabetic WT brains than in nondiabetic WT brains, whereas diabetic *Ppif* $^{-/-}$ brains showed lower EPR peaks, indicating much lower ROS levels in CypD-deficient brain tissues (Fig. 4*E* and *F*).

We further evaluated mitochondrial ROS generation by in situ staining with MitoSOX Red, a unique fluoroprobe highly selective for the detection of superoxide production in the mitochondria of live cells (41,45). The area occupied by MitoSOX Red staining in acute brain slices was significantly increased in the cerebral cortices and hippocampi of diabetic WT mice compared with nondiabetic WT controls. In contrast, diabetic *Ppif* $^{-/-}$ mice showed considerably less MitoSOX Red staining than diabetic WT mice (Fig. 4*G* and *H*). MitoSOX Red signals were extensively

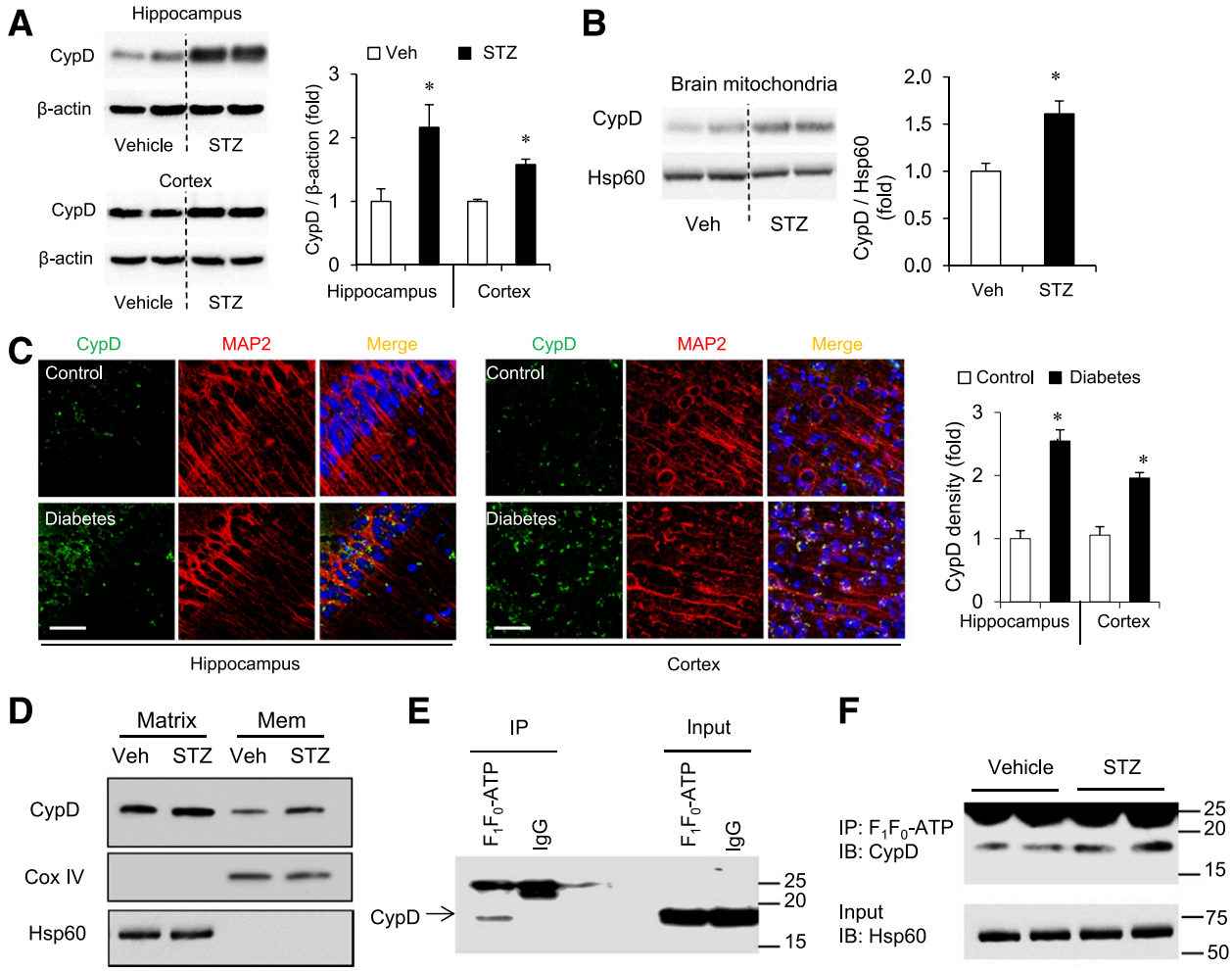

Figure 3—Elevated CypD expression induced increased CypD interaction with F_1F_0 ATP synthase in diabetic mitochondria. *A*: Immunoblotting and quantification of CypD protein levels in brain lysates from the hippocampus and cortex of control (veh) and STZ-induced diabetic mice. Data are represented as mean ± SEM (n = 6 mice per group). *$P < 0.05$. *B*: Immunoblotting and quantification of CypD protein levels normalized to Hsp60 in brain mitochondria. Data are represented as mean ± SEM (n = 3–5 mice per group). *$P < 0.05$. *C*: Quantification of the immunostaining intensity of CypD in the hippocampal CA1 region and cerebral cortex of control (veh) and STZ-induced diabetic mice. Cell body and dendrites of neurons were visualized by microtubule-associated protein 2 (MAP2). Scale bar, 50 μm. Data are represented as mean ± SEM (n = 5 mice per group). *$P < 0.05$. *D*: Immunoblotting of mitochondrial membranes (Mem) and matrix fractions from the indicated mice for CypD translocation assay. Cyclooxygenase (Cox) IV and Hsp60 served as mitochondrial membrane protein marker and matrix protein markers, respectively. *E*: Coimmunoprecipitation experiments showing CypD interaction with F_1F_0 ATP synthase. Mitochondrial lysates were immunoprecipitated (IP) with anti-ATP synthase antibody or IgG, followed by SDS-PAGE and immunodetection using anti-CypD antibody. *F*: CypD is increased in ATP synthase immunoprecipitates from STZ brain mitochondria. Immunoblotting (IB) analyses of input using anti-Hsp60 antibody confirm the equal amount of mitochondrial protein loading. Veh, vehicle.

colocalized with mitochondrial Hsp60, confirming the presence of mitochondria-derived ROS (Fig. 4*I*). Oxidative posttranslational protein modifications in the brain were assessed histochemically using antibody against 4-HNE, a major product of endogenous lipid peroxidation and a reliable marker of oxidative stress. Levels of 4-HNE were significantly decreased in the cortices of diabetic *Ppif* $^{-/-}$ mice compared with diabetic WT mice (Fig. 4*J*). Together, these data suggest that blockade of F_1F_0 ATP synthase–CypD interaction by genetic deletion of CypD confers protection against diabetes-induced mitochondrial respiratory deficits and oxidative stress in the brain.

CypD Deficiency Protects Against Diabetes-Induced Impairments in Spatial Learning and Memory and Synaptic Plasticity

To further determine whether CypD deficiency affords a protective effect on diabetes-induced cognitive decline, we used the MWM test to assess spatial learning and memory in STZ-induced diabetic WT and *Ppif* $^{-/-}$ mice. During the spatial acquisition phase, nondiabetic WT mice demonstrated a day-to-day decrease in escape latency, whereas diabetic WT mice exhibited longer escape latencies, suggesting impaired spatial learning (Fig. 5*A*). Compared with nondiabetic WT mice, diabetic mice crossed the platform location fewer times and spent significantly less time in

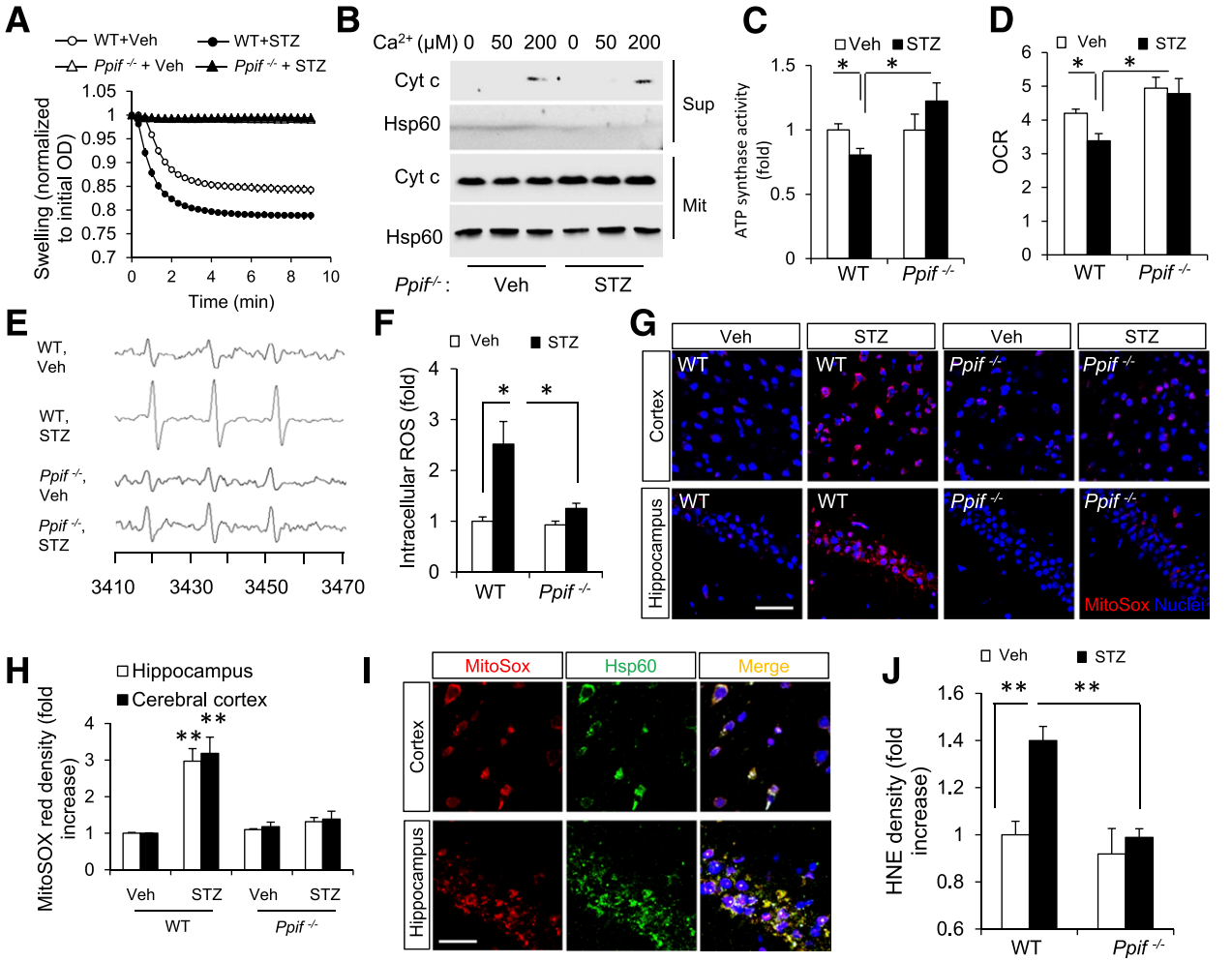

Figure 4—CypD deficiency rescues mitochondrial deficits in diabetic brains. *A*: Mitochondria lacking the gene encoding CypD (*Ppif*$^{-/-}$) are desensitized to 100 μmol/L Ca^{2+}-induced mitochondria swelling (n = 4–5 mice per group). *B*: CypD deficiency inhibited Ca^{2+}-induced cytochrome *c* (Cyt c) release. Isolated mitochondria were incubated with the indicated concentrations of Ca^{2+} for 30 min, and then the resultant supernatant (Sup) and pellets (Mit) were immunoblotted for cytochrome *c* and Hsp60. Hsp60 served as a control for an equivalent amount of the mitochondria in each sample and the mitochondrial protein marker. *C*: ATP synthase activity was restored by CypD deficiency in mouse brain. *D*: CypD deficiency prevents diabetes-induced OCR deficit (n = 4–8 mice for each group). *P < 0.05. *E* and *F*: Detection of ROS in cortical slices from indicated mice by using EPR spectra. The peak height indicates the level of ROS (n = 3–4 for the indicated group of mice). *P < 0.05. *G*: Representative fluorescent images of MitoSOX Red (red) staining in the cortex (top panels) and hippocampal CA1 region (bottom panels). Scale bar, 50 μm. *H*: Quantifications of MitoSOX Red staining intensity (n = 3 mice per group). **P < 0.01 vs. other groups of mice. *I*: Colocalization of MitoSOX (red) with Hsp-60 staining (green) in mitochondria of diabetic mice (overlay, yellow). Scale bar, 20 μm. *J*: Quantification of HNE staining intensity in brain sections (n = 3 mice per group). OD, optical density; Veh, vehicle. Data are represented as mean ± SEM. **P < 0.01.

the target quadrant during the probe test in which the escape platform was removed (Fig. 5*B*–*D*). Notably, the impairment in learning and memory exhibited by diabetic WT mice was ameliorated in diabetic *Ppif* $^{-/-}$ mice, as indicated by shorter escape latency, increased target quadrant occupation, and more target zone crossings (Fig. 5*A*–*D*). The performance of nondiabetic *Ppif* $^{-/-}$ mice did not differ from that of nondiabetic WT mice in the MWM test (Fig. 5*A*–*D*), suggesting that CypD deficiency has no effect on hippocampus-dependent spatial memory under physiological condition. There were no observable differences in swimming speed among the four groups of mice, indicating that the learning and memory improvement exhibited by *Ppif* $^{-/-}$ mice were not likely caused by differences in motor activity (Supplementary Fig. 4*A*).

To assess the effect of CypD deficiency on diabetes-induced synaptic dysfunction, we assessed hippocampal synaptic plasticity, which represents the molecular basis of new memory formation and is often assessed by LTP (46,47). Although LTP was significantly lower in diabetic WT mice, inhibition of CypD-involved mPTP opening by CsA significantly blocked LTP suppression in hippocampal slices from diabetic WT mice (Fig. 5*E* and *G*). Consistent with the results from spatial learning and memory performance, CypD deficiency restored LTP in diabetic mice (Fig. 5*F* and *G*). LTP was not altered in nondiabetic

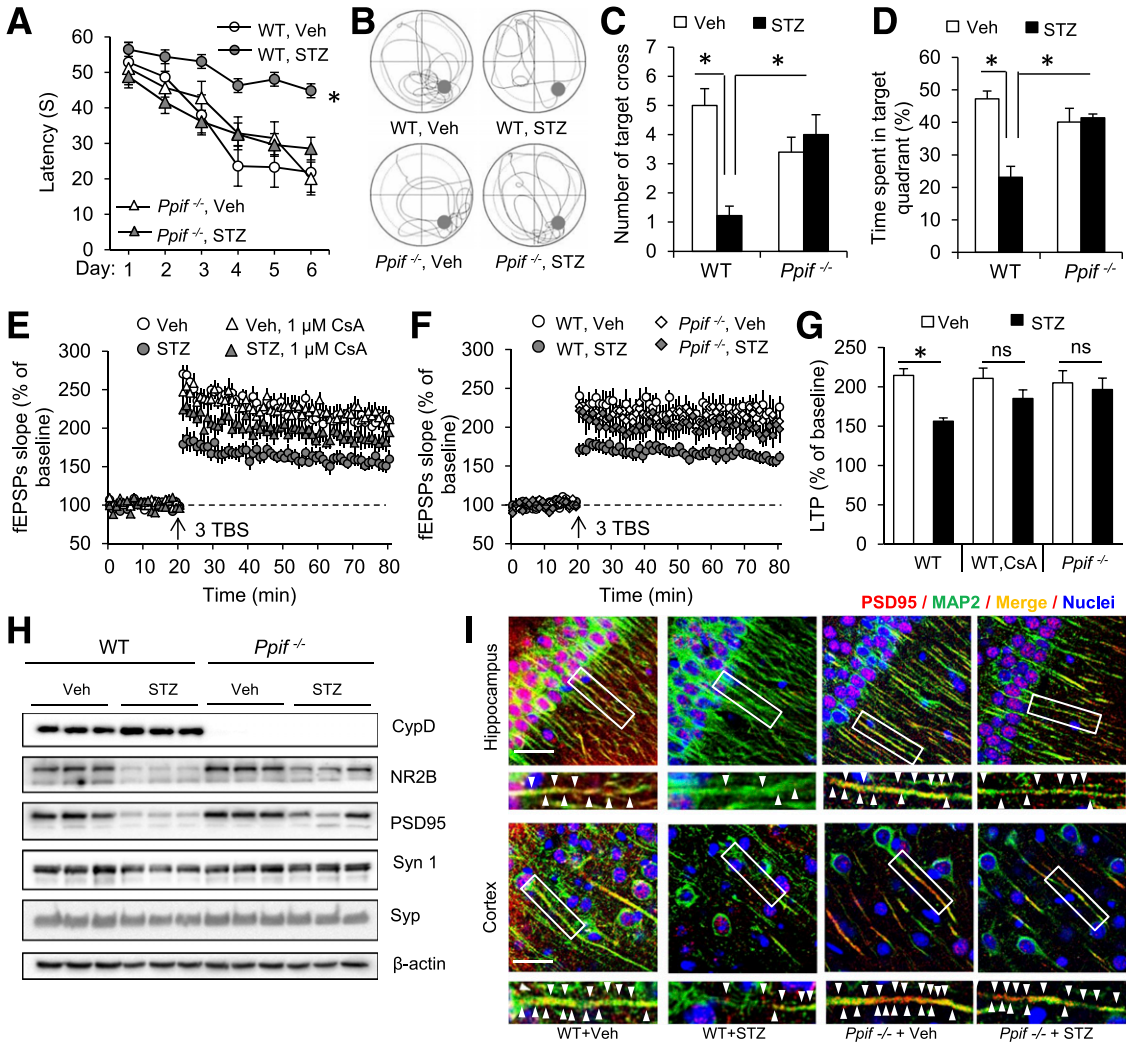

Figure 5—Protective effects of CypD deficiency on diabetes-induced impairment in learning and memory and synaptic dysfunction. *A–D*: Spatial memory was assessed by MWM testing in the indicated mice at 2–3 months after STZ injection (n = 5–9 mice per group). *A*: Escape latencies in hidden-platform test. *B*: Representative swimming paths during the probe trial on day 7. *C*: Number of platform location crossings during the probe trial. *D*: Time spent in the target quadrant during the probe trial. *$P < 0.05$. *E–G*: LTP was induced by θ-burst stimulation (TBS) 20 min after baseline recordings of SC-CA1 synapses in acute hippocampal slices from the indicated mice. LTP is expressed as the percentage of baseline (%). *E*: Inhibition of mPTP formation by CsA-rescued diabetes-induced decline in LTP. CsA (2 μmol/L) was added into the artificial cerebrospinal fluid before baseline recording and present for the duration of the LTP recording. *F*: Genetic deficiency of CypD rescued the decline in LTP in STZ-induced diabetic mice. fEPSPs, field-excitatory postsynaptic potentials. *G*: The magnitudes of LTP were measured 60 min after the TBS was given. Data are represented as mean ± SEM (n = 7–9 slices from n = 3–5 mice per group). *$P < 0.05$; ns: not significant. *H* and *I*: CypD deficiency reverses diabetes-induced synaptic loss. *H*: Immunoblots of brain homogenates for presynaptic (Syn 1, synapsin I; Syp, synaptophysin) and postsynaptic (NR2B and PSD95) protein expression in WT or *Ppif* $^{-/-}$ mice with indicated treatments. *I*: Expression of PSD95 in pyramid neurons in hippocampal CA1 region and cerebral cortex were visualized by immunohistochemical analysis. Cell bodies and dendrites of neurons were visualized by microtubule-associated protein 2 (MAP2). Higher magnification micrographs of the boxed regions are shown in the panels to the right. Scale bar, 50 μm. The arrowheads point to the PSD95-positive puncta on the dendrites of pyramid neurons. Veh, vehicle.

Ppif $^{-/-}$ mice (Fig. 5*F* and *G*). No changes in basal synaptic transmission were found in any mice groups (Supplementary Fig. 4*B*).

We next evaluated whether CypD-involved synaptic dysfunction was reflected in alterations in synaptic structure. To explore possible beneficial effects of CypD ablation on synaptic perturbation in the diabetes-affected brain, we measured expression levels of synapse-related proteins including post- and presynaptic proteins. Immunoblotting of brain homogenates revealed that levels of two major postsynaptic proteins, NR2B and PSD95, were significantly decreased in diabetic WT mice, whereas *Ppif* $^{-/-}$ mice displayed significantly restored levels of these two proteins (Fig. 5*H*). Levels of synapsin I and synaptophysin, which are both presynaptic proteins, were not significantly different between diabetic WT mice and nondiabetic WT mice (Fig. 5*H*). These results were further confirmed by in situ staining of PSD95 puncta in mouse brain sections.

Decreased amounts of PSD95-positive puncta on the dendrites of pyramidal neurons were observed in the cerebral cortex and hippocampus CA1 region in diabetic WT mice compared with nondiabetic WT mice (Fig. 5*I*). Notably, the number of PSD95-positive puncta was increased in diabetic *Ppif* $^{-/-}$ mice compared with diabetic WT mice (Fig. 5*I*). There was no difference in the quantity of synaptophysin-positive puncta in the cerebral cortex and hippocampus of diabetic mice compared with nondiabetic WT mice (Supplementary Fig. 5*A* and *B*). In addition, there was a slight but not significant decrease in the brain weight of diabetic mice compared with their nondiabetic counterparts (Supplementary Table 2), suggesting that the decreased synaptic protein level was unlikely due to global neuronal loss. Taken together, these behavioral, electrophysiological and biochemical studies indicate that blockade of F_1F_0 ATP synthase–CypD interaction by CypD ablation protects against diabetes-induced synaptic dysfunction and memory loss.

Increased Expression of CypD Is Associated With Cognitive Decline in Patients With Diabetes

To determine the correlation between CypD expression and diabetes-associated cognitive disorders, we evaluated the expression of CypD in brains from postmortem patients with diabetes by immunoblotting and immunohistochemistry. The study randomly selected 14 individuals (Supplementary Table 1) from subjects who had enrolled in the Brain and Body Donation Program of the Banner Sun Health Research Institute (33). These subjects received cognitive assessments until death, including Mini-Mental State Examination (MMSE) (48,49). Analysis of CypD protein levels using immunoblotting revealed significant increased expression of CypD in the inferior temporal cortex of the human brain samples (Fig. 6*A* and *B*), which correlates with MMSE scores. Analysis of CypD immunohistochemistry staining in the temporal cortex confirmed the negative correlation between MMSE scores and CypD expression (Fig. 6*C* and *D*). The difference in PMI between brain tissues from healthy control subjects and those from patients with diabetes was not statistically significant ($P > 0.05$) (Supplementary Table 1). These results suggest that the alternation in CypD expression levels is unlikely due to the variable degrees of autolysis of brain tissues.

DISCUSSION

Mitochondrial dysfunction and synaptic damage are pathological features of diabetes-affected brains (10,50–53). Diabetes imposes deleterious effects on the brain and increases the risk of depression, dementia, and cognitive decline (54,55). In neurons, mitochondria at synapses are vital for maintenance of synaptic function and transmission through normal mitochondrial dynamics, proper distribution and trafficking, energy metabolism, and synaptic Ca modulation. The perturbation of mitochondrial energy metabolism and the balance of mitochondrial dynamics contribute to alterations in mitochondrial structure and function induced by oxidative stress and hyperglycemia (10,40). In the current study, we have demonstrated for the first time the involvement of CypD-mediated mPTP formation in diabetes-induced brain mitochondrial and synaptic injury through F_1F_0 ATP synthase–CypD interaction in an STZ-induced diabetes mouse model. The STZ-induced diabetes mouse model is widely used for studying the mechanistic basis of diabetes-induced complications, including diabetic encephalopathy. Our previous and

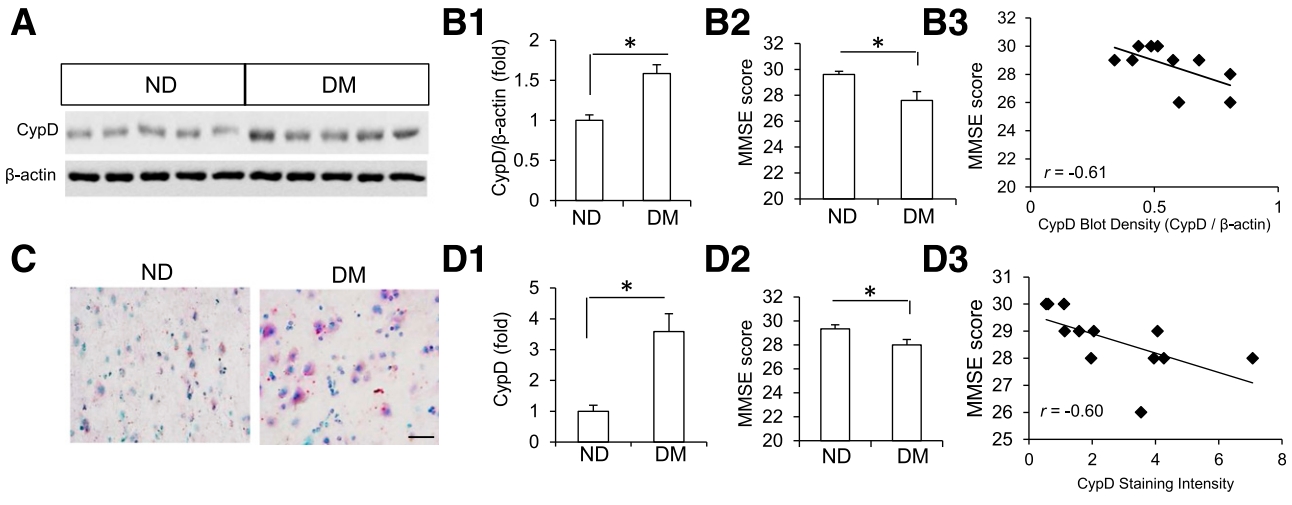

Figure 6—Correlation of CypD expression with cognitive decline in patients with diabetes. *A*: Immunoblotting analyses of CypD protein levels in brain samples from patients with diabetes (n = 5 for each group). *B1*: Quantification of CypD immunoreative bands relative to β-actin. *B2*: The comparison of MMSE score between nondiabetes controls (ND) and diabetic brains (DM). *B3*: Individual MMSE score (*y* axis) plotted against brain CypD levels (*x*-axis) detected by immunoblotting. CypD expression levels were normalized to β-actin levels. *$P < 0.05$. The Pearson correlation coefficient (r) is indicated. *C*: Representative images of CypD immunohistochemistry staining in the temporal cortex of human brains. Scale bar, 50 μm. *D1*: Quantification of CypD immunostaining intensity. *D2*: The comparison of MMSE score between ND and DM individuals. *D3*: Individual MMSE score (*y*-axis) plotted against CypD levels (*x*-axis) detected by immunohistochemical staining. The Pearson correlation coefficient (r) is indicated (n = 6 per group). *$P < 0.05$.

present studies have demonstrated that STZ-induced diabetic mice exhibit mitochondrial and synaptic abnormalities along with cognitive dysfunction, which reflect with cognitive decline in patients with diabetes (34). These data indicate the clinical relevance of the STZ-induced diabetes mouse model to human disease such as diabetes-involved CNS complications and dementia. Thus, our findings generated from *Ppif* $^{-/-}$ with STZ-induced diabetes provide substantial evidence that CypD/ATP synthase–mediated brain mitochondrial and synaptic pathology contributes to the cognitive decline and dementia that were seen in patients with diabetes.

Application of the single-channel patch clamp on the mitochondrial membrane revealed that diabetes specifically increased mPTP opening probability (P_0) in brain mitochondria. Consistent with this observation, isolated diabetic mitochondria displayed increased swelling and cytochrome *c* release during Ca^{2+} overload. These data indicate that diabetic brain mitochondria are hypersensitive to mPTP opening in response to stressors such as Ca^{2+} overload. Although the molecular properties of mPTP remain elusive, regulation of the mPTP in vivo and in vitro was extensively investigated. Matrix pH, membrane potential, oxidation-reduction state, Ca^{2+}, p53, as well as the Bax and Bcl-2 family could modulate mPTP opening (17,38,56–58). These modulations of mPTP opening are CypD-dependent because they can be blocked by CsA or CypD ablation (15,17,38), suggesting that CypD functions as a switch controlling the transition of mPTP from transient opening to prolonged opening in response to mitochondrial stress. The newly proposed mPTP model based on the F_1F_0 ATP synthase–CypD interaction provides more molecular detail of CypD-dependent mPTP regulation. The new model is further supported by our findings that interaction of CypD with ATP synthase correlates with increased expression of CypD in diabetes-affected mitochondria, which significantly elevates mPTP formation and aberrant mitochondrial function (mitochondrial swelling, cytochrome *c* release, energy deficiency, and oxidative stress) and suppresses ATP production in diabetes. Consequently, extensive ATP synthase–CypD interaction augments oxidative stress as shown by the protective effect of CypD deficiency against mitochondrial ROS accumulation and mitochondrial respiratory function, all in conjunction with the resistance of brain mitochondria to permeability transition. We therefore concluded that increased interaction of CypD with ATP synthase, resulting in increased mPTP opening and decreased ATP production, contributes to mitochondrial dysfunction in diabetic brains.

Furthermore, we demonstrated that blockade of the F_1F_0 ATP synthase–CypD interaction by deleting the binding partner CypD not only restored mitochondrial function but also alleviated deficits in synaptic plasticity and improved learning and memory insulted by diabetes. These observations are in line with the protective effect of suppression of CypD-mediated mPTP on Ca homeostasis, oxidative stress, and mitochondrial properties. Investigation of human brains affected by diabetes suggests that CypD elevation plays an important role in the mild cognitive dysfunction or early cognitive dysfunction in diabetes. This correlation between CypD expression and cognitive decline was also evident in STZ-induced diabetic mice. CypD expression was increased in the hippocampus and cerebellar cortex of diabetic brains, which expectedly displayed significant deficits in spatial memory and synaptic plasticity. Notably, CypD deficiency protected diabetic mice from synaptic plasticity deficits and spatial memory decline as well as restored synaptic proteins. Expression levels of CypD are significantly associated with mitochondrial properties, including the capacity for mPTP opening and mitochondrial function. Low expression of CypD in brain mitochondria increases resistance to mPTP opening induced by Ca (59), whereas high expression of CypD results in greater vulnerability to mPTP opening and higher required levels of CsA (an inhibitor of CypD) to inhibit mPTP opening (19,60,61). Importantly, elevated CypD expression levels observed in the temporal cortices of patients with diabetes and STZ-induced diabetic brains point to the clinical relevance of CypD in the pathogenesis of diabetes-involved neurodegeneration. The biochemical and functional data presented in our study reflect a causal link between CypD-mediated mitochondrial abnormalities and cognitive impairment relevant to diabetes.

Another potential mechanism underlying diabetes-induced mitochondrial and synaptic dysfunction in diabetic mice may be involved in amyloid-β (Aβ) accumulation in parallel with elevation of CypD expression. The interaction of Aβ with CypD elicits CypD-containing mPTP formation in an Aβ-enriched environment, consequently causing brain mitochondrial oxidative stress, mitochondrial swelling, synaptic injury, and cognitive impairment (19). Hyperglycemia could interfere with Aβ or amyloid precursor protein metabolism in diabetic transgenic mice overexpressing human amyloid precursor protein and Aβ (62–64), suggesting that diabetes exacerbates Alzheimer's disease–like pathology such as cerebral Aβ accumulation. However, compared with chronic diabetes with Aβ accumulation, no significant changes in Aβ levels were found in the acute STZ-induced diabetic brain compared with the vehicle-treated brain (34,50,65). Thus, the increased interaction of CypD with ATP synthase, caused by increased CypD expression, might represent an alternative molecular mechanism underlying cognitive dysfunction in diabetic encephalopathy and dementia.

In summary, our studies clearly demonstrate that lack of CypD remarkably improved cognitive and synaptic function in mice with STZ-induced type 1 diabetes. In the diabetes-affected brain, elevated CypD expression increases the interaction of CypD with ATP synthase, leading to mPTP opening, disruption of mitochondrial integrity, impairment of ATP production, and increased ROS generation. Notably, CypD ablation strengthens mitochondria against diabetes-induced mitochondrial and synaptic perturbation, at least in part, by maintaining

the integrity of mPTP, as shown by improved brain mitochondrial function and decreased ROS production, as well as by rescued synaptic plasticity and memory deficits in diabetic CypD knockout mice. Although the pathological events from an animal model of short-term untreated diabetes may not be comparable to that from years of diabetes or treated patients with diabetes, our findings clearly demonstrate that CypD is a mediator of diabetes-induced brain dysfunction, which provides a foundation for preclinical effect via targeting CypD/ATP synthase–perturbed mPTP as a potential therapeutic approach for diabetes-associated dementia and cognitive impairment, a medical condition for which few effective therapeutic options are currently available.

Funding. This study was supported by grants from the National Institute of Neurological Disorders and Stroke (R01-NS-089116) and National Institute on Aging (R37-AG-037319, R01-AG-044793). Support for the EPR instrumentation was provided by National Science Foundation Chemical Instrumentation Grant (0946883).

Duality of Interest. No potential conflicts of interest relevant to this article were reported.

Author Contributions. S.Y. designed and performed experiments, analyzed data, and wrote the paper. F.D. and Q.Y. performed experiments and analyzed data on mitochondrial function, EPR, and immunostaining. L.W. conducted the STZ injections and performed mouse behavioral tests. Z.Z. isolated the mitochondria and performed the mitochondrial swelling assay. C.Z. performed the coimmunoprecipitation assay. Y.W. assisted with the mitochondrial patch clamp, manuscript preparation, and discussion. L.-F.L. and D.G.W. provided the human tissues and the information of the case subjects. J.T.D. assisted with EPR experiments. S.S.Y. initiated and supervised the research, designed experiments, developed the concept, and wrote the paper. S.S.Y. is the guarantor of this work and, as such, had full access to all the data in the study and takes responsibility for the integrity of the data and the accuracy of the data analysis.

References

1. Huang CC, Chung CM, Leu HB, et al. Diabetes mellitus and the risk of Alzheimer's disease: a nationwide population-based study. PLoS One 2014;9:e87095
2. Ott A, Stolk RP, van Harskamp F, Pols HA, Hofman A, Breteler MM. Diabetes mellitus and the risk of dementia: The Rotterdam Study. Neurology 1999;53:1937–1942
3. Xu WL, Qiu CX, Wahlin A, Winblad B, Fratiglioni L. Diabetes mellitus and risk of dementia in the Kungsholmen project: a 6-year follow-up study. Neurology 2004;63:1181–1186
4. Sima AA. Encephalopathies: the emerging diabetic complications. Acta Diabetol 2010;47:279–293
5. Ferguson SC, Blane A, Wardlaw J, et al. Influence of an early-onset age of type 1 diabetes on cerebral structure and cognitive function. Diabetes Care 2005;28:1431–1437
6. Strachan MW, Reynolds RM, Marioni RE, Price JF. Cognitive function, dementia and type 2 diabetes mellitus in the elderly. Nat Rev Endocrinol 2011;7:108–114
7. Dietrich MO, Liu ZW, Horvath TL. Mitochondrial dynamics controlled by mitofusins regulate Agrp neuronal activity and diet-induced obesity. Cell 2013;155:188–199
8. del Carmen Ortiz C, Lores-Arnaiz S, Albertoni Borghese MF, et al. Mitochondrial dysfunction in brain cortex mitochondria of STZ-diabetic rats: effect of L-arginine. Neurochem Res 2013;38:2570–2580
9. Yang S, Xia C, Li S, Du L, Zhang L, Hu Y. Mitochondrial dysfunction driven by the LRRK2-mediated pathway is associated with loss of Purkinje cells and motor coordination deficits in diabetic rat model. Cell Death Dis 2014;5:e1217
10. Huang S, Wang Y, Gan X, et al. Drp1-mediated mitochondrial abnormalities link to synaptic injury in diabetes model. Diabetes 2015;64:1728–1742
11. Inoue I, Nagase H, Kishi K, Higuti T. ATP-sensitive K+ channel in the mitochondrial inner membrane. Nature 1991;352:244–247
12. Kirichok Y, Krapivinsky G, Clapham DE. The mitochondrial calcium uniporter is a highly selective ion channel. Nature 2004;427:360–364
13. Kinnally KW, Campo ML, Tedeschi H. Mitochondrial channel activity studied by patch-clamping mitoplasts. J Bioenerg Biomembr 1989;21:497–506
14. Nakagawa T, Shimizu S, Watanabe T, et al. Cyclophilin D-dependent mitochondrial permeability transition regulates some necrotic but not apoptotic cell death. Nature 2005;434:652–658
15. Baines CP, Kaiser RA, Purcell NH, et al. Loss of cyclophilin D reveals a critical role for mitochondrial permeability transition in cell death. Nature 2005;434:658–662
16. Murgia M, Rizzuto R. Molecular diversity and pleiotropic role of the mitochondrial calcium uniporter. Cell Calcium 2015;58:11–17
17. Vaseva AV, Marchenko ND, Ji K, Tsirka SE, Holzmann S, Moll UM. p53 opens the mitochondrial permeability transition pore to trigger necrosis. Cell 2012;149:1536–1548
18. Griffiths EJ, Halestrap AP. Protection by Cyclosporin A of ischemia/reperfusion-induced damage in isolated rat hearts. J Mol Cell Cardiol 1993;25:1461–1469
19. Du H, Guo L, Fang F, et al. Cyclophilin D deficiency attenuates mitochondrial and neuronal perturbation and ameliorates learning and memory in Alzheimer's disease. Nat Med 2008;14:1097–1105
20. Hou Y, Ghosh P, Wan R, et al. Permeability transition pore-mediated mitochondrial superoxide flashes mediate an early inhibitory effect of amyloid beta1-42 on neural progenitor cell proliferation. Neurobiol Aging 2014;35:975–989
21. Palma E, Tiepolo T, Angelin A, et al. Genetic ablation of cyclophilin D rescues mitochondrial defects and prevents muscle apoptosis in collagen VI myopathic mice. Hum Mol Genet 2009;18:2024–2031
22. Martin LJ, Semenkow S, Hanaford A, Wong M. Mitochondrial permeability transition pore regulates Parkinson's disease development in mutant α-synuclein transgenic mice. Neurobiol Aging 2014;35:1132–1152
23. Rasheed MZ, Tabassum H, Parvez S. Mitochondrial permeability transition pore: a promising target for the treatment of Parkinson's disease. Protoplasma 29 January 2016 [Epub ahead of print]. DOI: 10.1007/s00709-015-0930-2
24. Warne J, Pryce G, Hill JM, et al. Selective inhibition of the mitochondrial permeability transition pore protects against neurodegeneration in experimental multiple sclerosis. J Biol Chem 2016;291:4356–4373
25. Fujimoto K, Chen Y, Polonsky KS, Dorn GW 2nd. Targeting cyclophilin D and the mitochondrial permeability transition enhances beta-cell survival and prevents diabetes in Pdx1 deficiency. Proc Natl Acad Sci U S A 2010;107:10214–10219
26. Feng D, Tang Y, Kwon H, et al. High-fat diet-induced adipocyte cell death occurs through a cyclophilin D intrinsic signaling pathway independent of adipose tissue inflammation. Diabetes 2011;60:2134–2143
27. Taddeo EP, Laker RC, Breen DS, et al. Opening of the mitochondrial permeability transition pore links mitochondrial dysfunction to insulin resistance in skeletal muscle. Mol Metab 2013;3:124–134
28. Riojas-Hernández A, Bernal-Ramírez J, Rodríguez-Mier D, et al. Enhanced oxidative stress sensitizes the mitochondrial permeability transition pore to opening in heart from Zucker Fa/fa rats with type 2 diabetes. Life Sci 2015;141:32–43
29. Szabó I, Zoratti M. The giant channel of the inner mitochondrial membrane is inhibited by cyclosporin A. J Biol Chem 1991;266:3376–3379
30. Alavian KN, Beutner G, Lazrove E, et al. An uncoupling channel within the c-subunit ring of the F1FO ATP synthase is the mitochondrial permeability transition pore. Proc Natl Acad Sci U S A 2014;111:10580–10585
31. Giorgio V, Bisetto E, Soriano ME, et al. Cyclophilin D modulates mitochondrial F0F1-ATP synthase by interacting with the lateral stalk of the complex. J Biol Chem 2009;284:33982–33988
32. Giorgio V, von Stockum S, Antoniel M, et al. Dimers of mitochondrial ATP synthase form the permeability transition pore. Proc Natl Acad Sci U S A 2013;110:5887–5892

33. Beach TG, Sue LI, Walker DG, et al. The Sun Health Research Institute Brain Donation Program: description and experience, 1987-2007. Cell Tissue Bank 2008;9:229–245
34. Wang Y, Wu L, Li J, et al. Synergistic exacerbation of mitochondrial and synaptic dysfunction and resultant learning and memory deficit in a mouse model of diabetic Alzheimer's disease. J Alzheimers Dis 2015;43:451–463
35. Du H, Guo L, Yan S, Sosunov AA, McKhann GM, Yan SS. Early deficits in synaptic mitochondria in an Alzheimer's disease mouse model. Proc Natl Acad Sci U S A 2010;107:18670–18675
36. Ravera S, Panfoli I, Aluigi MG, Calzia D, Morelli A. Characterization of myelin sheath F(o)F(1)-ATP synthase and its regulation by IF(1). Cell Biochem Biophys 2011;59:63–70
37. Sayeed I, Parvez S, Winkler-Stuck K, et al. Patch clamp reveals powerful blockade of the mitochondrial permeability transition pore by the D2-receptor agonist pramipexole. FASEB J 2006;20:556–558
38. Karch J, Kwong JQ, Burr AR, et al. Bax and Bak function as the outer membrane component of the mitochondrial permeability pore in regulating necrotic cell death in mice. eLife 2013;2:e00772
39. Lustbader JW, Cirilli M, Lin C, et al. ABAD directly links Abeta to mitochondrial toxicity in Alzheimer's disease. Science 2004;304:448–452
40. Gan X, Wu L, Huang S, et al. Oxidative stress-mediated activation of extracellular signal-regulated kinase contributes to mild cognitive impairment-related mitochondrial dysfunction. Free Radic Biol Med 2014;75:230–240
41. Mukhopadhyay P, Rajesh M, Haskó G, Hawkins BJ, Madesh M, Pacher P. Simultaneous detection of apoptosis and mitochondrial superoxide production in live cells by flow cytometry and confocal microscopy. Nat Protoc 2007;2:2295–2301
42. Yan S, Li Z, Li H, Arancio O, Zhang W. Notoginsenoside R1 increases neuronal excitability and ameliorates synaptic and memory dysfunction following amyloid elevation. Sci Rep 2014;4:6352
43. Zhang H, Wang Y, Yan S, et al. Genetic deficiency of neuronal RAGE protects against AGE-induced synaptic injury. Cell Death Dis 2014;5:e1288
44. De Filippis B, Valenti D, de Bari L, et al. Mitochondrial free radical overproduction due to respiratory chain impairment in the brain of a mouse model of Rett syndrome: protective effect of CNF1. Free Radic Biol Med 2015;83:167–177
45. Fang D, Wang Y, Zhang Z, et al. Increased neuronal PreP activity reduces Aβ accumulation, attenuates neuroinflammation and improves mitochondrial and synaptic function in Alzheimer disease's mouse model. Hum Mol Genet 2015;24:5198–5210
46. Ho VM, Lee JA, Martin KC. The cell biology of synaptic plasticity. Science 2011;334:623–628
47. Bliss TV, Collingridge GL. A synaptic model of memory: long-term potentiation in the hippocampus. Nature 1993;361:31–39
48. Tombaugh TN, McIntyre NJ. The Mini-Mental State Examination: a comprehensive review. J Am Geriatr Soc 1992;40:922–935
49. Folstein MF, Folstein SE, McHugh PR. "Mini-mental state". A practical method for grading the cognitive state of patients for the clinician. J Psychiatr Res 1975;12:189–198
50. Guo Y, Wang P, Sun H, Cai R, Xia W, Wang S. Advanced glycation end product-induced astrocytic differentiation of cultured neurospheres through inhibition of Notch-Hes1 pathway-mediated neurogenesis. Int J Mol Sci 2013;15:159–170
51. Schmidt RE, Parvin CA, Green KG. Synaptic ultrastructural alterations anticipate the development of neuroaxonal dystrophy in sympathetic ganglia of aged and diabetic mice. J Neuropathol Exp Neurol 2008;67:1166–1186
52. Li XL, Aou S, Oomura Y, Hori N, Fukunaga K, Hori T. Impairment of long-term potentiation and spatial memory in leptin receptor-deficient rodents. Neuroscience 2002;113:607–615
53. Stranahan AM, Arumugam TV, Cutler RG, Lee K, Egan JM, Mattson MP. Diabetes impairs hippocampal function through glucocorticoid-mediated effects on new and mature neurons. Nat Neurosci 2008;11:309–317
54. Crane PK, Walker R, Hubbard RA, et al. Glucose levels and risk of dementia. N Engl J Med 2013;369:540–548
55. Yaffe K, Lindquist K, Schwartz AV, et al. Advanced glycation end product level, diabetes, and accelerated cognitive aging. Neurology 2011;77:1351–1356
56. Petronilli V, Cola C, Bernardi P. Modulation of the mitochondrial cyclosporin A-sensitive permeability transition pore. II. The minimal requirements for pore induction underscore a key role for transmembrane electrical potential, matrix pH, and matrix Ca2+. J Biol Chem 1993;268:1011–1016
57. Petronilli V, Costantini P, Scorrano L, Colonna R, Passamonti S, Bernardi P. The voltage sensor of the mitochondrial permeability transition pore is tuned by the oxidation-reduction state of vicinal thiols. Increase of the gating potential by oxidants and its reversal by reducing agents. J Biol Chem 1994;269:16638–16642
58. Bernardi P, Rasola A, Forte M, Lippe G. The mitochondrial permeability transition pore: channel formation by F-ATP synthase, integration in signal transduction, and role in pathophysiology. Physiol Rev 2015;95:1111–1155
59. Eliseev RA, Filippov G, Velos J, et al. Role of cyclophilin D in the resistance of brain mitochondria to the permeability transition. Neurobiol Aging 2007;28:1532–1542
60. Hajnóczky G, Hoek JB. Cell signaling. Mitochondrial longevity pathways. Science 2007;315:607–609
61. Du H, Guo L, Zhang W, Rydzewska M, Yan S. Cyclophilin D deficiency improves mitochondrial function and learning/memory in aging Alzheimer disease mouse model. Neurobiol Aging 2011;32:398–406
62. Chao AC, Lee TC, Juo SH, Yang DI. Hyperglycemia Increases the production of amyloid beta-peptide leading to decreased endothelial tight junction. CNS Neurosci Ther 2016;22:291–297
63. Macauley SL, Stanley M, Caesar EE, et al. Hyperglycemia modulates extracellular amyloid-β concentrations and neuronal activity in vivo. J Clin Invest 2015;125:2463–2467
64. Takeda S, Sato N, Uchio-Yamada K, et al. Diabetes-accelerated memory dysfunction via cerebrovascular inflammation and Abeta deposition in an Alzheimer mouse model with diabetes. Proc Natl Acad Sci U S A 2010;107:7036–7041
65. Burdo JR, Chen Q, Calcutt NA, Schubert D. The pathological interaction between diabetes and presymptomatic Alzheimer's disease. Neurobiol Aging 2009;30:1910–1917